Supplementary Materials

Direct observation of contact resistivity for monolayer TMD based junctions *via* PL spectroscopy

Linglong Zhang,[1]*🡻 Yilin Tang,[2]* Han Yan,[3]* Tanju Yildirim,[4] Shunshun Yang,[1] Haizeng Song,[5] Xiaowei Zhang,[6] Fuguo Tian[1], Zhongzhong Luo,[7] Jiajie Pei,[8] Qi Yang,[9] Yixin Xu,[1] Xiaoying Song,[10] Ahmed Raza Khan,[2,11] Sihao Xia,[1] Xueqian Sun,[2] Bo Wen,[12]🡻 Fei Zhou,[13,14]🡻 Weiwei Li,[1]🡻 Youwen Liu[1], Han Zhang[9]

[1]College of Physics, Nanjing University of Aeronautics and Astronautics, Key Laboratory of Aerospace Information Materials and Physics (NUAA), MIIT, Nanjing 211106, China

[2]Research School of Engineering, College of Engineering and Computer Science, The Australian National University, Canberra, ACT, 2601, Australia

[3]Department of Materials Science and Metallurgy, University of Cambridge, Cambridge CB3 0FS, UK

[4]Center for Functional Sensor & Actuator (CFSN), National Institute for Materials Science (NIMS), Tsukuba, Ibaraki 305-0044, Japan

[5]School of Electronic Science and Engineering, Nanjing University, Nanjing 210093, China

[6]Department of Electrical Engineering and Computer Science, Ningbo University, Ningbo 315211, China

[7]College of Electronic and Optical Engineering & College of Flexible Electronics (Future Technology)，Jiangsu Province Engineering Research Center for Fabrication and Application of Special Optical Fiber Materials and Devices，Nanjing University of Posts and Telecommunications，9 Wenyuan Road, Nanjing, Jiangsu 210023, China

[8]College of Materials Science and Engineering, Fuzhou University, Fuzhou 350108, Fujian, China
[9]Collaborative Innovation Center for Optoelectronic Science and Technology, International Collaborative Laboratory of 2D Materials for Optoelectronic Science and Technology of Ministry of Education and Guangdong Province, Shenzhen University, Shenzhen, 518060, China
[10]College of Optoelectronic Engineering, Chongqing University of Posts and Telecommunications, Chongqing, China.
[11]Department of Industrial and Manufacturing Engineering University of Engineering and Technology (Rachna College) Lahore 54700, Pakistan
[12]Institute of Nanosurface Science and Engineering, Guangdong Provincial Key Laboratory of Micro/Nano Optomechatronics Engineering, Shenzhen University, Shenzhen 518060, China
[13]National Key Laboratory for Precision Hot Processing of Metals; School of Materials Science and Engineering, Harbin Institute of Technology, Harbin 150001, China.
[14]State Key Laboratory for Environment-friendly Energy Materials, School of Materials Science and Engineering, Southwest University of Science and Technology, Mianyang, 621010, China
*These authors contributed equally to this work.
🡻E-mail: linglongzhang1@126.com, Bo Wen (dr.bowen1986@outlook.com), Fei Zhou (angel.flyfly@hotmail.com), Weiwei Li (wl337@nuaa.edu.cn)

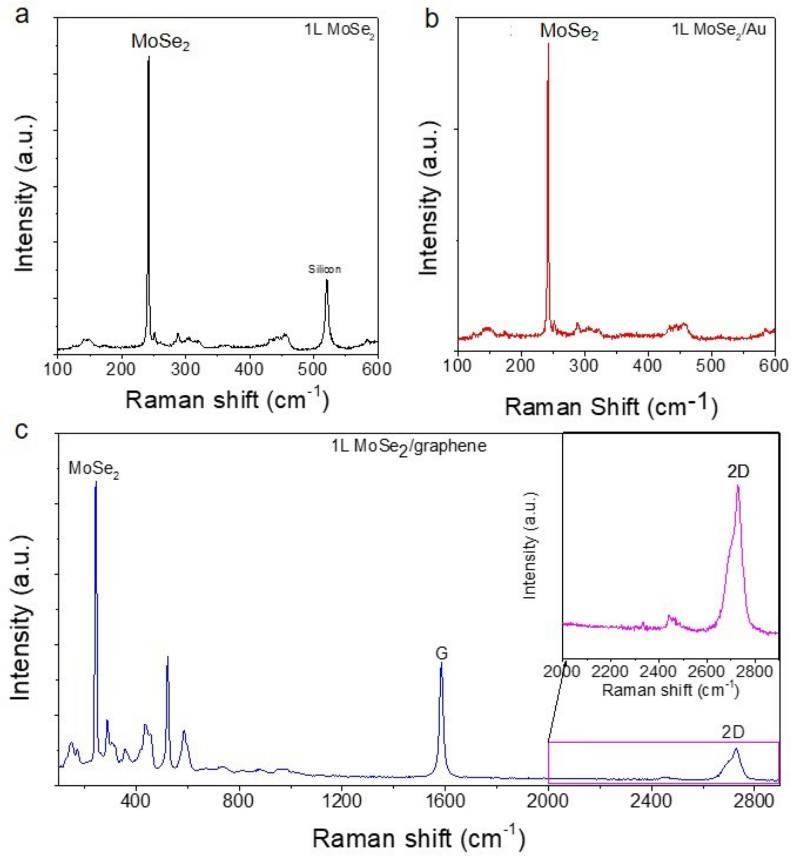

Figure S1 Confirmation of the structures of individual 1L $MoSe_2$, 1L $MoSe_2$/Au and 1L $MoSe_2$/graphene. a-c Raman spectra of 1L $MoSe_2/SiO_2$ (a) and 1L $MoSe_2$/Au (b) and 1L $MoSe_2$/graphene structures (c) at room temperature. The inset in (c) shows the Zoom in Raman spectrum of the selected region. The Raman active modes consist well with the reported monolayer $MoSe_2$ and 2D graphene crystals.[1,2]

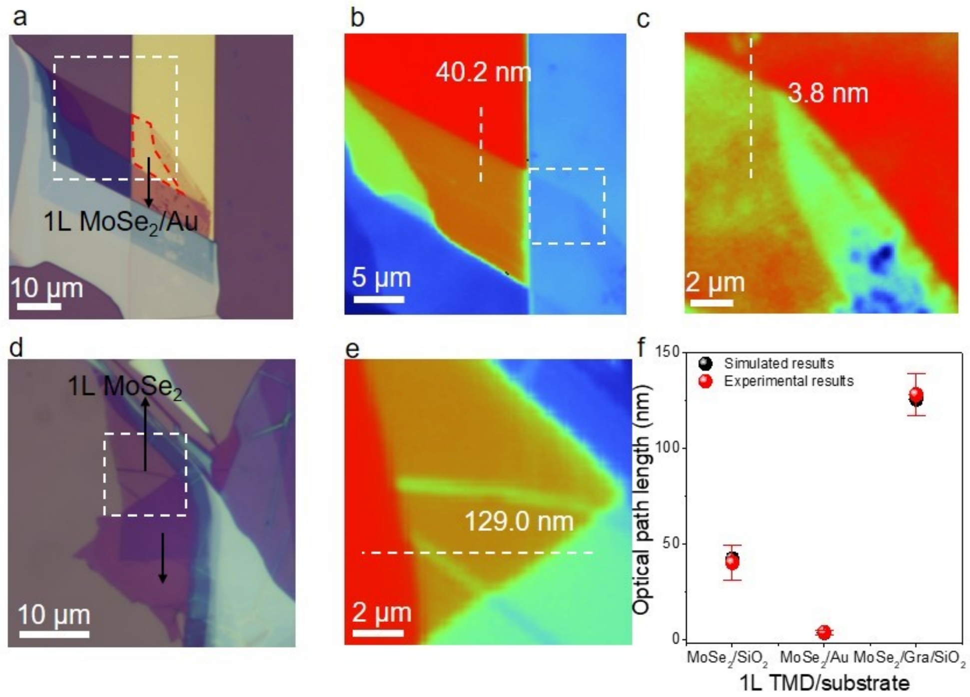

Figure S2 PSI characterizations of different structures a, Optical image of 1L $MoSe_2/SiO_2$ and 1L $MoSe_2$/Au structures. Scale bar is 10 μm. **b,** PSI images of 1L $MoSe_2/SiO_2$ corresponding to the dashed line region in (a). Scale bar is 5 μm. **c,** PSI images of 1L $MoSe_2$/Au structures corresponding to the dashed line region in (b). Scale bar is 2 μm. **d**, Optical image of 1L $MoSe_2/SiO_2$ and 1L $MoSe_2$/graphene structures. Scale bar is 10 μm. **e,** PSI images of 1L $MoSe_2$/graphene structures corresponding to the dashed line regions in (d), where the thickness of graphene is around 10 nm. Scale bar is 2 μm. **f,** Experimental statistics and simulation data representations of the optical path lengths (OPL) from monolayer $MoSe_2$ on the various substrates. The values were then used to calibrate the thickness of monolayer $MoSe_2$ using at least two sets of measurements on each sample.[3,4] Red spheres show the experimental data and black spheres show the simulated results.

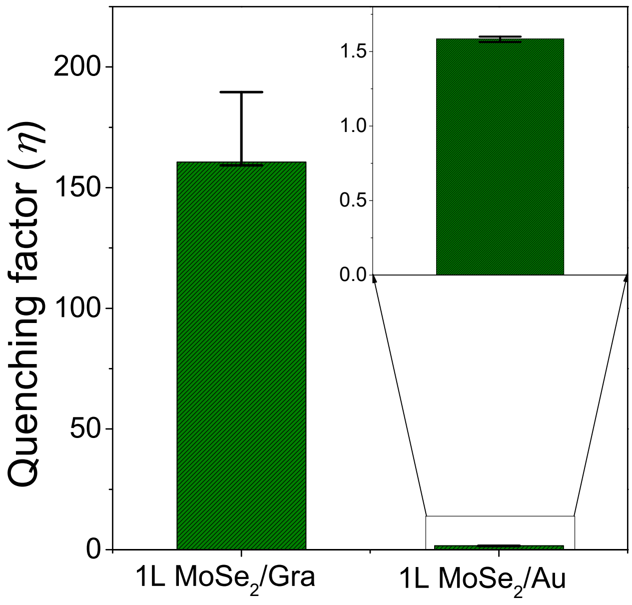

Figure S3 Error analyses of quenching factors for both junctions. *Experimental statistics of the quenching factor from 1L MoSe$_2$/graphene and 1L MoSe$_2$/Au junctions at room temperature.*

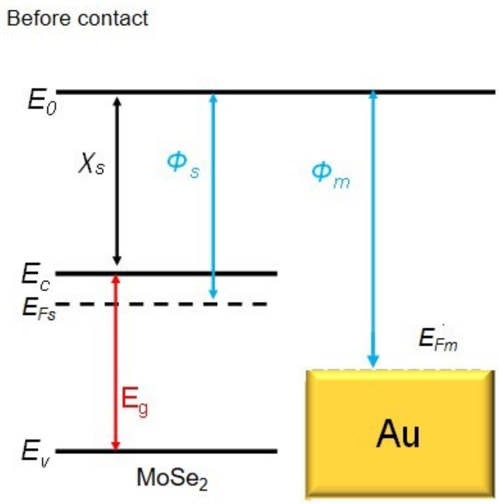

Figure S4 The electrical band alignment of 1L $MoSe_2$/Au junctions before contact. The electrical band alignment of monolayer $MoSe_2$ and gold electrode before contact, showing that it is n-type material with a higher Fermi level than the gold.

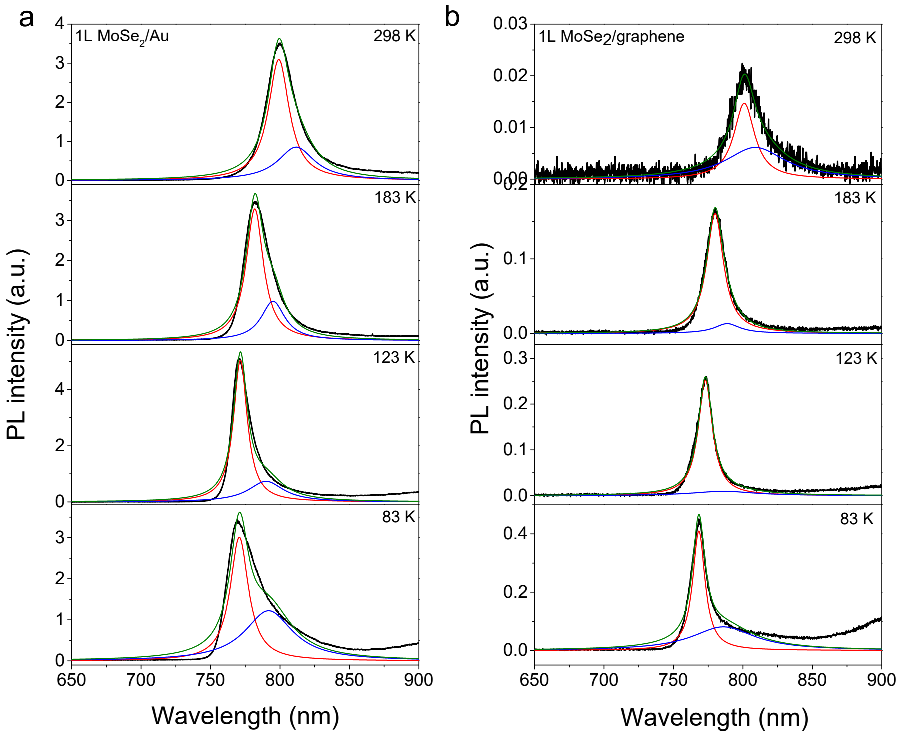

Figure S5 PL spectra fitting. a, The PL spectra fittings for 1L $MoSe_2$/Au at the temperature from 298 K to 83 K. **b**, The PL spectra fittings for 1L $MoSe_2$/graphene as a function of temperature. The PL spectra were fitted by Lorenz functions (Black lines were the experimental data, Red lines were labeled as Fit Peak 1 representing A exciton peak, blue lines were labeled as Fit Peak 2 representing T trion peak, and olive lines were labeled as Cumulative Fit.)

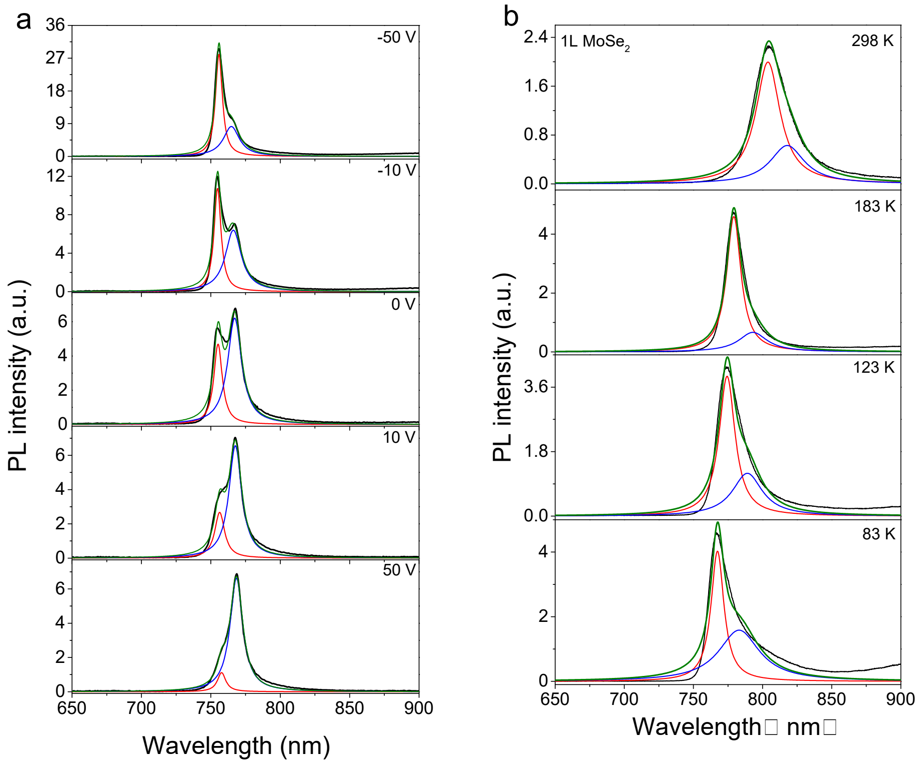

Figure S6 PL spectra fittings. a, The PL spectra fittings for 1L $MoSe_2$/Au at the back gate voltages from -50 V to 50 V. **b**, The PL spectra fittings for 1L $MoSe_2$ as a function of temperature. The PL spectra were fitted by Lorenz functions (Black lines were the experimental data, Red lines were labeled as Fit Peak 1 representing A exciton peak, blue lines were labeled as Fit Peak 2 representing T trion peak, and olive lines were labeled as Cumulative Fit.)

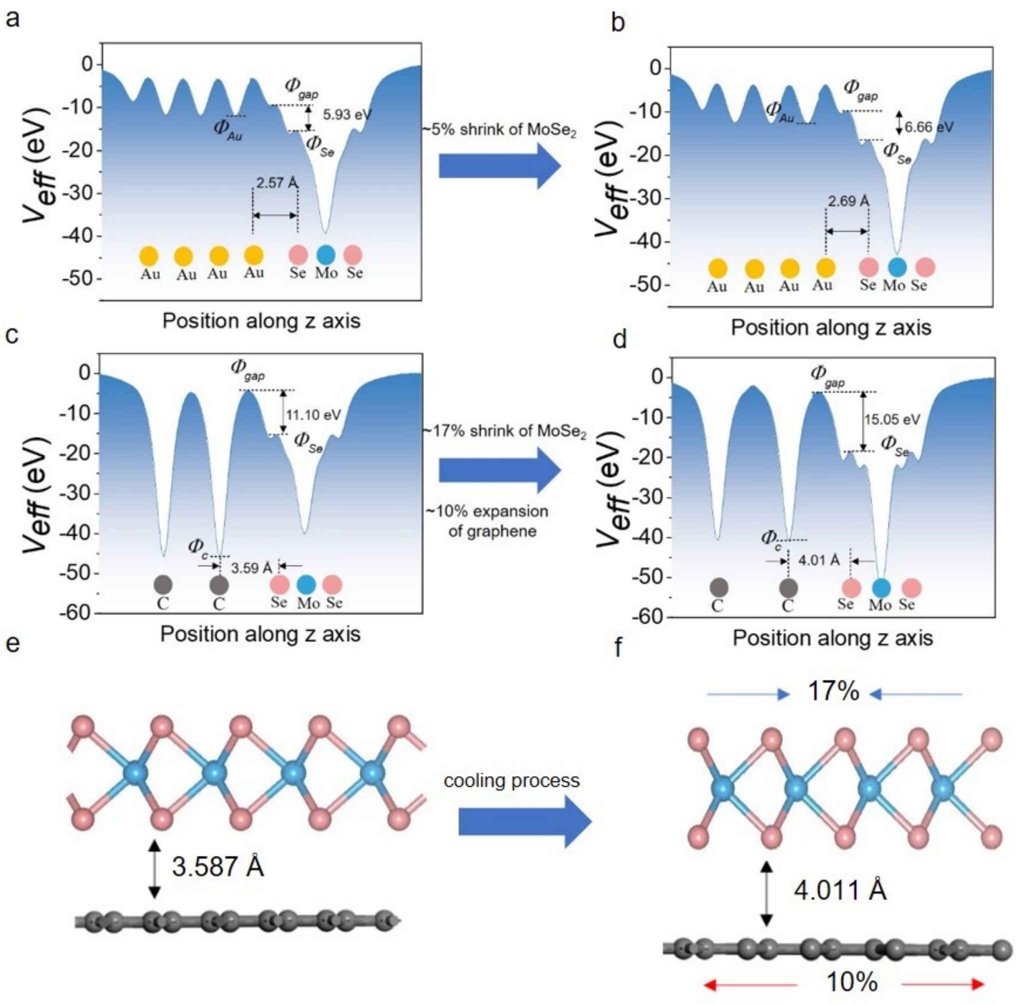

Figure S7 Evaluation of the tunnel barrier change with lattice strains. **a,** Plot of minimum effective potential (V_{eff}) versus z position for Au-$MoSe_2$ top contact. **b,** The barrier changes of Au-$MoSe_2$ model with ~ 5% lateral shrink of $MoSe_2$ lattice. The barriers increase from 5.93 eV to 6.66 eV. **c,** Plot of V_{eff} versus z position for bilayer graphene-$MoSe_2$ top contact. **d,** The barrier changes of the graphene-$MoSe_2$ model with ~17% lateral shrink of $MoSe_2$ lattice and ~ 10% lateral expansion of graphene lattice. The barriers increase from 11.10 eV to 15.05 eV. **e,f** Simulated interlayer spacing change under the reverse strain during cooling process.

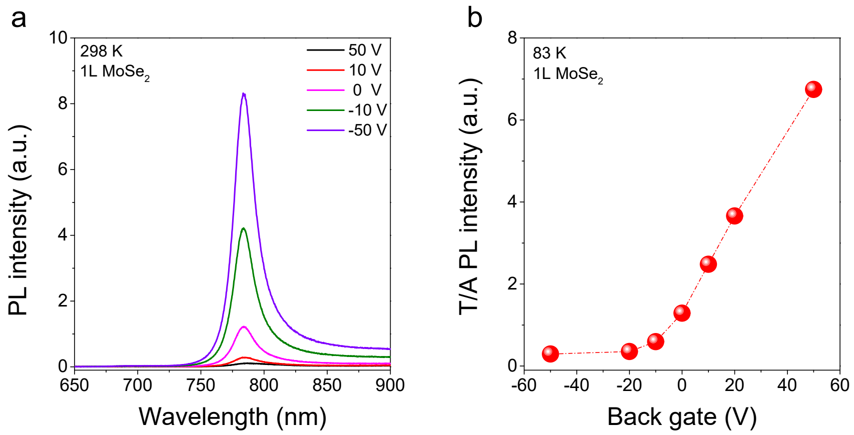

Figure S8 Exciton and trion dynamics in monolayer $MoSe_2$. a, PL intensity of 1L $MoSe_2$ as a function of back gate voltage at room temperature. **b**, T/A PL intensity of 1L $MoSe_2$ as a function of back gate voltages at 83 K, confirming the temperature-induced doping effects.

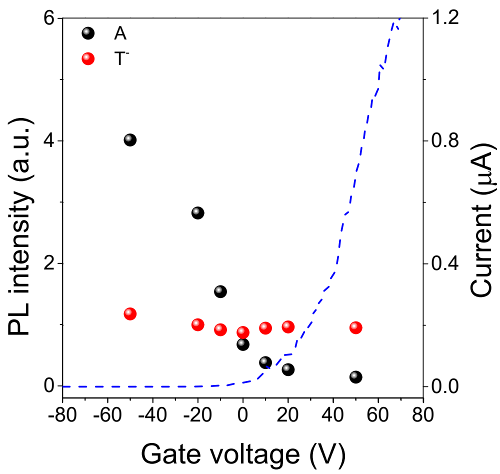

Figure S9 Exciton and trion dynamics in monolayer $MoSe_2$. PL intensity of A and T (left) and the drain-source current (right) as a function of back gate voltages from 1L $MoSe_{2,}$ showing that the charge neutral point is at ~-60 V.

Supplementary Note S1: Thickness characterizations by using PSI

It was accepted that the phase-shift interferometry (PSI) system could measure the optical path length (OPL) of 2D materials.[5] The OPL is determined through the equation: $OPL_i = -\frac{\lambda}{2\pi}(\emptyset_i - \emptyset_{sub})$, where λ is the wavelength of the light source (i.e., 535 nm), $\emptyset_i$ and $\emptyset_{sub}$ represent the measured phase shifts of the reflected light signal from the monolayer TMD and the substrate respectively.[6] The corresponding measured OPL values of 1L $MoSe_2$ on SiO_2, 1L$MoSe_2$ on Au and 1L$MoSe_2$ on graphene and SiO_2 substrates are 40.2, 3.8, 129.0 nm, respectively (Figure S2). Moreover, we performed the numerical simulation based on the Stanford stratified Structure Solver (S4)[7] to calculate the OPL values for monolayer $MoSe_2$ on the aforementioned substrates (Figure S2e). In the calculations the refractive index values of SiO_2, Si, 1L $MoSe_2$, graphene and Au are set to 1.46[8], 4.15+0.05i[9,10], 5.6+1.8i,[11] 2.6-1.3i,[6] 0.54+2.21i,[12] respectively. The measured and simulated *OPL* values consist well with each other (Figure S2).

Supplementary Note S2: Photoexcited current

After contact, the position of Fermi level (E_{Fs}) shifts towards the middle of the $MoSe_2$ band gap (E_i) and then reaches the equilibrium state with the same Fermi level with gold due to contact dopings.[13,14] As shown in Figure 1d, the shifted Fermi level (E_{Fs}) indicates that monolayer $MoSe_2$ on gold is still n-type after the contact, which is consistent with the subsequent gate-dependent PL measurements and theoretical predictions.[13,15,16] During the PL measurements, photo-excited carriers would further shift the Fermi level of 1L $MoSe_2$ towards E_i, reaching a new quasi-fermi level (E_{Fd}). The Fermi level difference (ΔE_F), equivalent to an applied voltage in the electrostatic doping process, would continually cause the charge transfer from the TMD side to the interface. Meanwhile, photo-excited holes would be annihilated in the interface by the electrons from gold. The fast interfacial charge transfer between gold and $MoSe_2$ would form a current and lead to PL quenchings.[5,17-21]

Supplementary Note S3: Thermal expansion coefficients (TEC) mismatch-induced interlayer spacing changes

To understand why the quenching factor η in 1L $MoSe_2$/graphene decreases abruptly, the temperature-induced lattice changes were simulated by DFT. Because the graphene has a negative TEC and the $MoSe_2$ has a positive TEC,[22,23] the 2D lattice would experience a large structural change. For the clear demonstrations, we assumed the 10% expansion of graphene and 17% shrink of $MoSe_2$ and this leads to an increase in separation distance (*i.e.*, interlayer spacing) of ~ 12%. These changes trigger an increase in Φ_{gap} (Figure S7), which is beneficial to the decrease of quenching factor with temperatures. In addition, the quenching factor and interlayer spacing of $MoSe_2$/Au junction present a similar temperature-dependent tendency with that of $MoSe_2$/graphene junction (Figure S7 and 4b) although they are relatively weaker. These are possibly ascribed to the intrinsic effective potential difference ($\Phi_{barrier}$) in the former and temperature-induced doping effects.

Supplementary Note S4: Confirmation of charge neutrality for monolayer $MoSe_2$.

According to the I-V curves (Figure S9), we measured the charge neutrality point at -80 V corresponding to E_F=0 V, which consists well with the reported. Moreover, these results are quite consistent with gate-dependent PL measurements at room temperature and 83 K. At room temperature, while sweeping the back gate voltage from -50 V to 50 V, PL intensity decreases dramatically, exhibiting $MoSe_2$ is an n-type material. In contrast, PL spectra shape and intensity change considerably while sweeping the back gate voltage from -50 V to 50 V (Figure 5a and S8a). The corresponding Lorentz fittings demonstrate that the PL intensity ratio of trions to excitons firstly decreases abruptly from 50 V to 20 V and then remains constant from ~-20 V to -50 V. This indirectly proves the voltage for the charge neutrality point (Figure S8b).

Supplementary Note S5: Estimation of temperature-induced dopings.

To analyze the effect of temperature on the doping level, we calculated the dopings of monolayer $MoSe_2$ at temperatures varying from 298 K to 83 K. Based on the equation: $\Delta n=2m_eq^2\Delta E_F/\hbar^2\pi$，using the same electron effective mass of 1L $MoSe_2$ as in the main text, it could be calculated that the Fermi level shift of 15.5 meV induced by temperature in Figure 5 lead to a doping density of 6.4×10^{12} cm^{-2}. For comparisons, the photodoping density was calculated as well. In the experiments, we measured PL spectra of all structures under the excitation power of 43.8 μW (532 nm CW laser, laser beam size of 1 μm^2). The used fast decay lifetime of 1L $MoSe_2$ is 36.0 ps, which was extracted from a previously reported value.[1] According to the reported absorption (A) value of ~15.3%,[1] the absorbed photon number is calculated as $N = \frac{\sim 43.8\ \mu W * 36.0\ ps}{photon\ energy} * A$.[6] For simplification, each of the absorbed photons is assumed to create one hole-electron pair. Therefore, the photoexcited doping n in the 1L $MoSe_2$ was measured to be 6.47×10^{10} cm^{-2}. Since the temperature-induced dopings are two orders of magnitude higher than photo-doping densities, they can not be neglected in the analysis of contact resistance changes.

Consequently, the PL intensity of monolayer $MoSe_2$ will decrease as the temperature decreases. In contrast, the PL intensity of two junctions remains the same due to the contact with graphene or gold substrates. According to the equation: $\eta = I_{MoSe_2}/I_j$, the η will decrease with the decreasing temperature, which matches well with the observations in Figure 4b(I).

Supplementary Note S6: The effect of orbital overlaps on contact resistances

By DFT calculations, the band structures of 1L $MoSe_2$/Au and 1L $MoSe_2$/graphene junctions were compared (Figure 5e,f). The original band structure of the individual 1L $MoSe_2$ was presented for references (red curves). It can be clearly observed that a strong orbital hybridization occurs between $MoSe_2$ and gold. These state overlaps of Mo and Se and gold in the original band gap of $MoSe_2$ indicate the appearance of the covalent bands (Figure 5e). In contrast, in 1L $MoSe_2$/graphene junctions the band structure of $MoSe_2$ bands remains the same as that of the isolated

$MoSe_2$, indicating the lack of orbital overlaps (Figure 5d-f). On the other hand, after annealing process the *d* would experience a tiny change as the temperature decreases. This would significantly influence the R_C of 1L $MoSe_2$/Au instead of 1L $MoSe_2$/graphene junctions, owing to the absence of orbital overlaps in the latter. Hence, it confirms the explanation that a larger evolution of R_C in 1L $MoSe_2$/Au with temperature is attributed to orbital overlap modulations.[13,14]

References

1 Zhang, L. *et al.* Efficient and layer-dependent exciton pumping across atomically thin organic-inorganic type-I heterostructures. *Adv. Mater.* **30**, 1803986 (2018).

2 Liu, X. *et al.* Epitaxial ultrathin organic crystals on graphene for high-efficiency phototransistors. *Adv. Mater.* **28**, 5200-5205 (2016).

3 Sharma, A. *et al.* Defect engineering in few-layer phosphorene. *Small* **14**, 1704556 (2018).

4 Tongay, S. *et al.* Defects activated photoluminescence in two-dimensional semiconductors: Interplay between bound, charged, and free excitons. *Sci. Rep.* **3**, 2657 (2013).

5 Xu, R. *et al.* Layer-dependent surface potential of phosphorene and anisotropic/layer-dependent charge transfer in phosphorene-gold hybrid systems. *Nanoscale* **8**, 129-135 (2016).

6 Yang, J. *et al.* Optical tuning of exciton and trion emissions in monolayer phosphorene. *Light Sci. Appl.* **4**, e312 (2015).

7 Liu, V. *et al*. A free electromagnetic solver for layered periodic structures. *Comput. Phys. Commun.* **183**, 2233-2244 (2012).

8 Malitson, I. H. Interspecimen comparison of the refractive index of fused silica. *J. Opt. Soc. Am.* **55**, 1205-1209 (1965).

9 Aspnes, D. E. *et al*. Dielectric functions and optical parameters of Si, Ge, GaP, GaAs, GaSb, InP, InAs and InSb from 1.5 to 6.0 eV. *Phys. Rev. B* **27**, 985-1009 (1983).

10 Kim, J. H. *et al*. Polarized light scattering by dielectric and metallic spheres on silicon wafers. *Appl. Opt.* **41**, 5405-5412 (2002).

11 Hsu, C. *et al.* Thickness-dependent refractive index of 1L, 2L and 3L MoS_2, $MoSe_2$, WS_2 and WSe_2. *Adv. Opt. Mater.* **7**, 1900239 (2019).

12 Johnson, P. B. *et al*. Optical constants of the noble metals. *Phys. Rev. B* **6**, 4370-4379 (1972).

13 McDonnell, S. *et al*. Defect-dominated doping and contact resistance in MoS_2. *ACS Nano* **8**, 2880-2888 (2014).

14 Kang, J. *et al*. Computational study of metal contacts to monolayer transition-metal dichalcogenide semiconductors. *Phys. Rev. X* **4**, 031005 (2014).

15 Kaushik, N. *et al.* Schottky barrier heights for Au and Pd contacts to MoS_2. *Appl. Phys. Lett.* **105**, 113505 (2014).

16 Wang, Y. *et al.* Does p-type ohmic contact exist in WSe_2-metal interfaces? *Nanoscale* **8**, 1179-1191 (2016).

17 Homan, S. B. *et al.* Ultrafast exciton dissociation and long-lived charge separation in a photovoltaic pentacene MoS_2 van der Waals heterojunction. *Nano Lett.* **17**, 164-169 (2016).

18 Currie, M. *et al*. Optical control of charged exciton states in tungsten disulfide. *Appl. Phys. Lett.* **106**, 201907 (2015).

19 Tongay, S. *et al.* Broad-range modulation of light emission in two-dimensional semiconductors by molecular physisorption gating. *Nano Lett.* **13**, 2831-2836 (2013).
20 Wang, X. H. *et al.* Photoinduced doping and photoluminescence signature in an exfoliated WS_2 monolayer semiconductor. *RSC Adv.* **6**, 27677-27681 (2016).
21 Zongyou Yin *et al.* Single-layer MoS_2 phototransistors. *ACS Nano* **6**, 74-80 (2012).
22 El-Mahalawy, S. H. *et al*. The Thermal Expansion of 2H-MoS_2, 2H-$MoSe_2$ and 2H-WSe_2 between 20 and 800°C. *J Appl. Crystallogr.* **9**, 403-406 (1976)
23 Yoon, D. *et al*. Negative thermal expansion coefficient of graphene measured by Raman spectroscopy. *Nano Lett.* **11**, 3227-3231 (2011).